Quantitative optical coherence tomography angiography of vascular abnormalities in the living human eye

Yali Jia[a], Steven T. Bailey[a], Thomas S. Hwang[a], Scott M. McClintic[a], Simon S. Gao[a], Mark E. Pennesi[a], Christina J. Flaxel[a], Andreas K. Lauer[a], David J. Wilson[a], Joachim Hornegger[b], James G. Fujimoto[c], and David Huang[a,1]

[a]Casey Eye Institute, Oregon Health & Science University, Portland, OR 97239; [b]Pattern Recognition Lab and School of Advanced Optical Technologies, University Erlangen-Nuremberg, D-91058 Erlangen, Germany; and [c]Department of Electrical Engineering and Computer Science and Research Laboratory of Electronics, Massachusetts Institute of Technology, Cambridge, MA 02139

Edited by Morton Goldberg, The Johns Hopkins Wilmer Eye Institute, Baltimore, MD, and accepted by the Editorial Board March 26, 2015 (received for review January 6, 2015)

Retinal vascular diseases are important causes of vision loss. A detailed evaluation of the vascular abnormalities facilitates diagnosis and treatment in these diseases. Optical coherence tomography (OCT) angiography using the highly efficient split-spectrum amplitude decorrelation angiography algorithm offers an alternative to conventional dye-based retinal angiography. OCT angiography has several advantages, including 3D visualization of retinal and choroidal circulations (including the choriocapillaris) and avoidance of dye injection-related complications. Results from six illustrative cases are reported. In diabetic retinopathy, OCT angiography can detect neovascularization and quantify ischemia. In age-related macular degeneration, choroidal neovascularization can be observed without the obscuration of details caused by dye leakage in conventional angiography. Choriocapillaris dysfunction can be detected in the nonneovascular form of the disease, furthering our understanding of pathogenesis. In choroideremia, OCT's ability to show choroidal and retinal vascular dysfunction separately may be valuable in predicting progression and assessing treatment response. OCT angiography shows promise as a noninvasive alternative to dye-based angiography for highly detailed, in vivo, 3D, quantitative evaluation of retinal vascular abnormalities.

optical coherence tomography angiography | ophthalmic imaging | ocular circulation

Optical coherence tomography (OCT) has become the most commonly used imaging modality in ophthalmology. It provides cross-sectional and 3D imaging of the retina and optic nerve head with micrometer-scale depth resolution. Structural OCT enhances the clinician's ability to detect and monitor fluid exudation associated with retinal vascular diseases. Whereas anatomical alterations that impact vision are readily visible, structural OCT has a limited ability to image the retinal or choroidal vasculatures. Furthermore, it is unable to directly detect capillary dropout or pathologic new vessel growth (neovascularization) that are the major vascular changes associated with two of the leading causes of blindness, age-related macular degeneration (AMD) and diabetic retinopathy (1). To visualize these changes, traditional i.v. contrast dye-based angiography techniques are currently used.

Fluorescein dye is primarily used to visualize the retinal vasculature. A separate dye, indocyanine green (ICG), is necessary to evaluate the choroidal vasculature. Both fluorescein angiography (FA) and ICG angiography require i.v. injection, which is time consuming, and which can cause nausea, vomiting, and, rarely, anaphylaxis (2). Dye leakage or staining provides information regarding vascular incompetence (e.g., from abnormal capillary growth), but it also obscures the image and blurs the boundaries of neovascularization. Additionally, conventional angiography is 2D, which makes it difficult to distinguish vascular abnormalities within different layers. Therefore, it is desirable to develop a no-injection, dye-free method for 3D visualization of ocular circulation.

In recent years, several OCT angiography methods have been developed to detect changes in the OCT signal caused by flowing red blood cells in blood vessels. Initially, Doppler OCT angiography methods were investigated for the visualization and measurement of blood flow (3–8). Because Doppler OCT is only sensitive to motion parallel to the OCT probe beam, it is limited in its ability to image retinal and choroidal circulations, which are predominantly perpendicular to the OCT beam. More recent approaches, based on detecting variation in the speckle pattern over time, are sensitive to both transverse and axial flow. Several types of speckle-based techniques have been described, including amplitude-based (9–11), phase-based (12), or a combination of both amplitude and phase (13) variance methods.

We developed an amplitude-based method called split-spectrum amplitude-decorrelation angiography (SSADA). The SSADA algorithm detects motion in the blood vessel lumen by measuring the variation in reflected OCT signal amplitude between consecutive cross-sectional scans. The novelty of SSADA lies in how the OCT

Significance

Retinal vascular diseases are a leading cause of blindness. Optical coherence tomography (OCT) has become the standard imaging modality for evaluating fluid accumulation in these diseases and for guiding treatment. However, fluorescein angiography (FA) is still required for initial evaluation of retinal ischemia and choroidal neovascularization, which are not visible in conventional structural OCT. The limitations of FA include poor penetration of fluorescence through blood and pigment, inability to determine the depth of the pathology due to its two-dimensional nature, and some uncommon but potentially severe complications. As a noninvasive three-dimensional alternative, OCT angiography may be used in routine screening and monitoring to provide new information for clinical diagnosis and management.

Author contributions: Y.J., S.T.B., T.S.H., M.E.P., C.J.F., A.K.L., D.J.W., and D.H. designed research; J.H. and J.G.F. contributed new reagents/analytic tools; Y.J., S.T.B., T.S.H., S.M.M., S.S.G., M.E.P., C.J.F., A.K.L., D.J.W., and D.H. analyzed data; and Y.J., S.T.B., T.S.H., S.M.M., S.S.G., M.E.P., and D.H. wrote the paper.

Conflict of interest statement: Oregon Health & Science University (OHSU), Y.J., J.G.F., and D.H. have a significant financial interest in Optovue, Inc., a company that may have a commercial interest in the results of this research and technology. These potential conflicts of interest have been reviewed and managed by OHSU. J.G.F. and D.H. receive royalties on an optical coherence tomography patent licensed by the Massachusetts Institute of Technology (MIT) to Carl Zeiss Meditec. J.G.F. and J.H. receive royalties from intellectual property owned by MIT and licensed to Optovue, Inc. Other authors do not have financial interest in the subject of this article.

This article is a PNAS Direct Submission. M.G. is a guest editor invited by the Editorial Board.

[1]To whom correspondence should be addressed. Email: huangd@ohsu.edu.

signal is processed to enhance flow detection and reject axial bulk motion noise. Compared with the full-spectrum amplitude method, SSADA using fourfold spectral splits improved the signal-to-noise ratio (SNR) by a factor of two, which is equivalent to reducing the scan time by a factor of four (14). More recent SSADA implementations use even more than a fourfold split to further enhance the SNR of flow detection. This highly efficient algorithm generates high-quality angiograms of both the retina and choroid. The angiograms have capillary-level detail and can be obtained with currently available commercial OCT systems.

This article uses six illustrative cases and highlights the various types of vascular pathologies that can be detected and measured using SSADA and an OCT angiography system of visualization. Additionally, we describe techniques designed to help clinicians rapidly interpret OCT angiograms and to easily identify pathological vascular features. These techniques include (*i*) separation of the 3D angiogram into individual vascular beds via segmentation algorithms, (*ii*) presentation of en face OCT angiograms, analogous to traditional angiography, (*iii*) creation of cross-sectional structural OCT images with superimposed OCT angiograms to help correlate anatomical alterations with vascular abnormalities, and (*iv*) quantification of neovascularization and capillary dropout in both the retinal and choroidal circulation.

Results

Retinal and Choroidal Microcirculation in Normal Subjects. The retina and choroid are two distinct vascular beds. The 3D nature of OCT angiography allows separate visualizations of these two circulations from the same volumetric scan. In healthy eyes, retinal circulation is located between the internal limiting membrane (ILM) and the outer plexiform layer (OPL), whereas the choroidal circulation is beneath Bruch's membrane (BM). The vitreous (anterior to the ILM) and outer retina (between OPL and Bruch's membrane) are avascular in normal eyes. One way to present OCT angiography is to use different colors, each representing different vascular beds, superimposed on gray-scale, cross-sectional, structural OCT images (Fig. 1*A*). Using this technique, both blood flow and retinal structural information are presented on a single image.

En face presentation of OCT angiography is comparable to the traditional view of dye-based angiography and is necessary for clinicians to identify vascular patterns. Segmented en face OCT angiograms can be displayed as individual retinal and choroidal circulations (Fig. 1 *C* and *E*). In healthy eyes, the vitreous and outer retinal layers are colored black (Fig. 1 *B* and *D*), representing the absence of flow.

In vivo imaging of the choroid is limited with current imaging modalities (15). High-quality OCT angiograms of the choriocapillaris can be obtained by segmenting a thin slice (10 μm) of the inner choroid below Bruch's membrane (Fig. 1*E*). The larger and deeper choroidal vessels are more difficult to visualize with SSADA-based OCT angiography because choriocapillaris flow causes a flow projection artifact in the deeper layers. Selective removal of this artifact is impossible, given the near confluent nature of the choriocapillaris. Another reason is that high flow in the larger choroidal vessels reduces the OCT signal due to interference fringe washout. However, visualization of the larger, deeper choroidal vessels is possible using an inverse reflectance display scale (Fig. 1*F*). This en face choroidal image is achieved by taking advantage of the OCT signal void produced by interference fringe washout in regions of very high flow velocity (16).

Retinal Neovascularization and Capillary Dropout in Diabetic Retinopathy. Diabetic retinopathy is a microangiopathy characterized by capillary occlusion, hyperpermeability, and neovascularization (17). These pathophysiologic changes cause proliferative diabetic retinopathy and macular edema, which are responsible for most of the vision loss associated with this disease (18). Assessment of the microvascular changes with FA has been validated as a way to classify disease severity and predict progression (19).

Like FA, OCT angiography can visualize areas of low capillary perfusion or dropout. Fig. 2 compares en face retinal OCT angiograms from a normal subject to those from a patient with nonproliferative diabetic retinopathy (NPDR). The central 0.6-mm

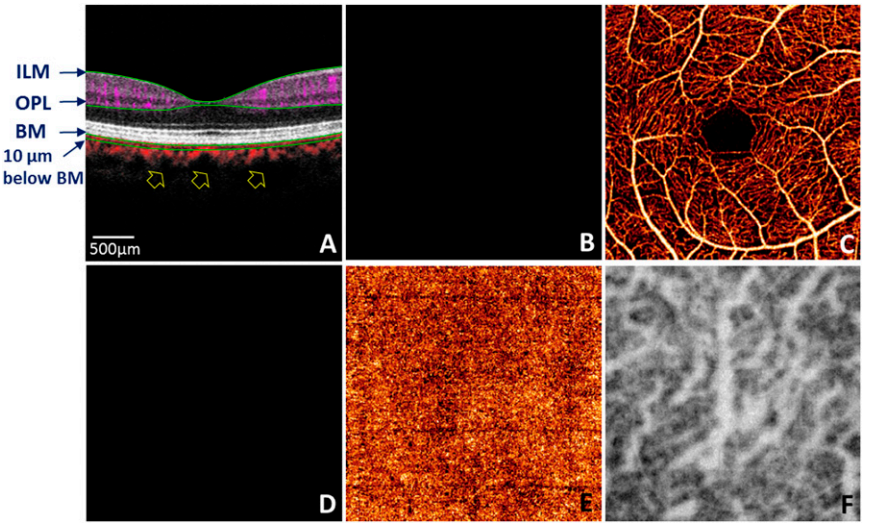

Fig. 1. Optical coherence tomography (OCT) angiography (3 × 3 mm) of a healthy human eye, acquired using a 70-kHz spectral OCT system with an 840-nm center wavelength. (*A*) Cross-sectional composite OCT angiogram. Depth layer segmentation lines are shown in green. BM, Bruch's membrane; ILM, internal limiting membrane; OPL, outer plexiform layer. Flow signals are color coded by depth: purple, anterior to the OPL; red, posterior to BM. (*B*) En face OCT angiogram above the ILM shows the normal, avascular vitreous. (*C*) En face OCT angiogram between the ILM and OPL shows the normal retinal vasculature. (*D*) En face OCT angiogram between the OPL and BM shows the normal, avascular outer retina. (*E*) En face OCT angiogram of the inner 10 μm of the choroid shows dense, relatively even flow throughout the central macula (3 × 3 mm). (*F*) En face OCT structural image with an inverse gray scale shows the deeper choroid with medium- and large-sized vessels.

circle encompasses the normal foveal avascular zone (FAZ), and areas of capillary loss are represented by dark areas elsewhere in the macula. No dark areas are present outside of the FAZ in the normal subject (Fig. 2 *B1*, *C1*, and *D1*), whereas the patient with NPDR has enlargement of the normal FAZ and extensive loss of the macular capillary bed (Fig. 2*B2*). Nonperfusion areas on FA correspond to those on OCT angiography (Fig. 2 *B2* and *C2*).

SSADA also enables the quantitative evaluation of local circulation by determining the flow index and vessel density in areas of interest, such as the parafoveal and perifoveal areas that correspond respectively to the 3-mm and 6-mm early treatment diabetic retinopathy study (ETDRS) macular fields (as demonstrated in Fig. 2) (19). Nonperfusion maps may be created (Fig. 2 *D1* and *D2*) that allows for the area of nonperfusion to be calculated and compared between sequential angiograms.

The development of retinal neovascularization (RNV) signifies progression to the proliferative phase of the disease. Recognition of this change is important because it may guide panretinal photocoagulation and other treatments to reduce the risk of vision loss due to RNV (20). Because OCT angiograms can be segmented by anatomic planes such as the ILM, it can be particularly effective in distinguishing between intraretinal microvascular abnormalities, which occur in the same plane as the retinal blood vessels, and early RNV, which develops anterior to the retinal vessels and may extend into the vitreous cavity (Fig. 3). The extent and viability of RNV can also be quantified on OCT angiography by vessel area and flow index. Thus, compared with FA, OCT angiography has the advantages of 3D localization and quantification.

Choroidal Neovascularization in Age-Related Macular Degeneration. Choroidal neovascularization (CNV), the hallmark pathologic feature of neovascular AMD, consists of abnormal blood vessels that grow from the choriocapillaris and penetrate through Bruch's membrane into the subretinal pigment epithelium (sub-RPE) space and subretinal space. Subsequent exudation and hemorrhage damage retinal tissue, resulting in vision loss (21). FA is the gold standard for CNV diagnosis (22); however, it is limited by its 2D nature. In addition, blocked fluorescence from the RPE or hemorrhage (if present) reduces visibility of the CNV beneath the RPE, as well as visualization of the choroid (23). OCT angiography has the capability to generate 3D angiograms of the retina, choroid, and CNV that is otherwise obscured in FA by RPE blockage or hemorrhage.

In an example of neovascular AMD (Fig. 4*A*), the late FA image (Fig. 4*B*) shows a stippled hyperfluoresence leakage pattern, indicating the presence of an occult CNV. The outer retina is devoid of blood flow in healthy eyes, and the flow detected in this area is associated with the presence of CNV. Color-coded composite en face OCT angiography allows for 3D representation of retinal flow, outer retinal flow, and choroidal flow on a single 2D image. In this case, the CNV is highlighted in yellow, and the extent and microvascular structure (Fig. 4*C*) is better defined compared with traditional FA image (Fig. 4*B*). The cross-sectional structural OCT image with a color-coded OCT angiogram overlay (Fig. 4*D*) demonstrates the depth of the CNV, in this case beneath the RPE, as well as the presence of fluid exudation and disruption of outer retinal anatomy.

This case illustrates the capability of OCT angiography to assess the morphology, extent, and depth of CNV in AMD. We have demonstrated that OCT angiography can be used to classify CNV as type I (between the RPE and Bruch's membrane, Fig. 4*D*), type II (above the RPE), type III (in the inner retina), or a combined type (24). OCT angiography can furthermore provide

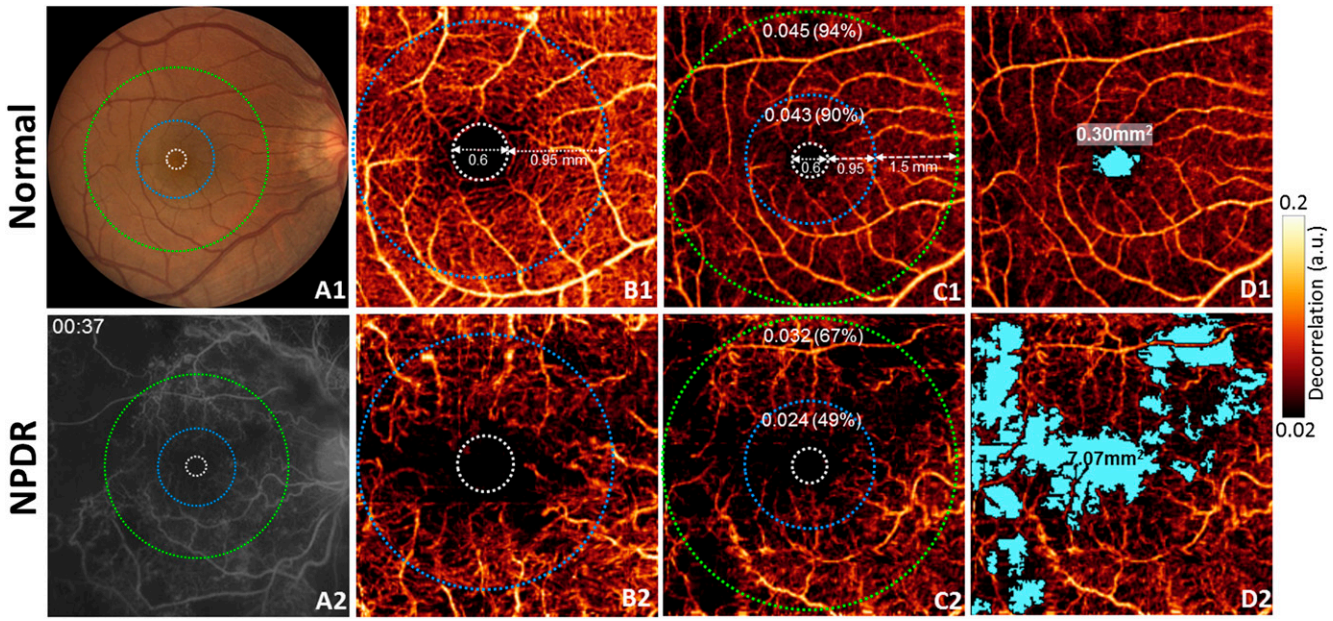

Fig. 2. Quantification of inner retinal blood flows in normal control (*A1–D1*) and nonproliferative diabetic retinopathy (NPDR) with macular edema (*A2–D2*). OCT angiography was acquired using a 70-kHz spectral OCT system with a center wavelength of 840 nm. White dashed circle indicates normal foveal avascular zone (FAZ, 0.6 mm diameter white dashed circle). Area between white and blue dashed circles indicates parafoveal zone. Area between blue and green dashed circles indicates perifoveal zone. First column (*A1* and *A2*) indicates fundus photo (*A1*) and fluorescein angiography (*A2*). Second column (*B1* and *B2*) indicates en face 3 × 3 mm OCT angiograms. Enlargement of the FAZ is present in the parafoveal region for NPDR (*B2*). Parafoveal and perifoveal retinal flow indexes (vessel densities) are shown on en face 6 × 6 mm OCT angiograms (*C1* and *C2*). Nonperfusion areas (blue) are shown of 6 × 6 mm OCT angiograms (*D1* and *D2*). The normal subject had a FAZ of 0.30 mm^2, whereas the NPDR case showed an enlarged FAZ and scattered areas of macular nonperfusion totaling 7.07 mm^2. Decorrelation (shown by the scale bar) as calculated by the SSADA algorithm measures fluctuation in the backscattered OCT signal amplitude (intensity). It is linear to blood flow velocity up to a saturation limit after which it reaches a maximum value. The linear range is approximately within the limits of capillary flow velocity.

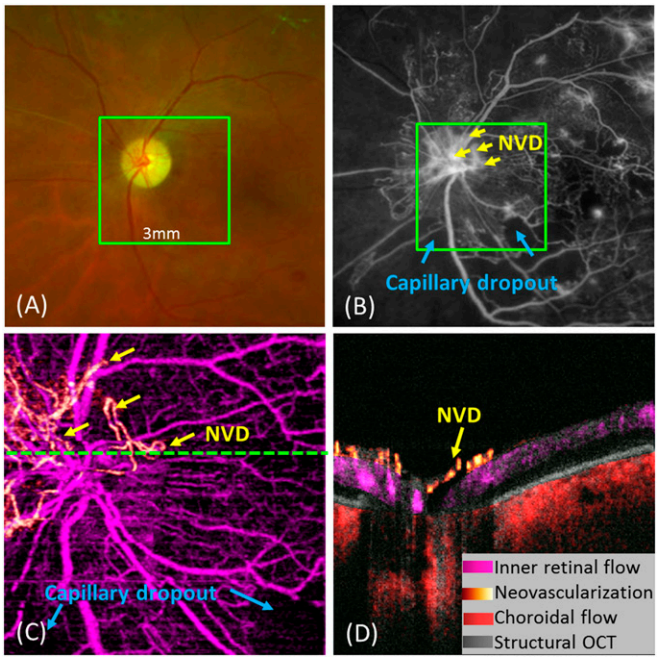

Fig. 3. Proliferative diabetic retinopathy (PDR) case imaged using a 100-kHz swept-source OCT system with a center wavelength of 1,050 nm. (*A*) Confocal scanning laser ophthalmoscope (cSLO) shows retinal neovascularization at the optic disk (NVD) and attenuated retinal vessels. (*B*) FA showing NVD and peripapillary capillary dropout. The green squares in *A* and *B* outline the 3 × 3 mm area shown on the OCT angiogram below. (*C*) En face OCT angiography showing NVD and areas of capillary dropout that correspond to FA (NV is shown in light red gold; normal retinal vessels are in purple). The area of NVD was 0.47 mm^2. The vitreous flow index was 0.022. (*D*) Cross-sectional composite OCT angiogram showing NVD above the inner limiting membrane (red/gold).

quantitative data regarding CNV flow and area. These capabilities may prove to be valuable in the assessment of disease severity and monitoring of the effectiveness of treatment. It is likely that, in many cases, CNV growth through Bruch's membrane occurs before the onset of exudation and visual symptoms. Whereas visual acuity at presentation is strongly predictive of the posttreatment outcome (25), OCT angiography may enable the detection of CNV before the development of symptoms or detectable changes with structural OCT or FA. Because it is a safe, noninvasive, and rapid imaging technique, at-risk patients may benefit from OCT angiography screening.

Choriocapillaris Loss in Age-Related Macular Degeneration. The choriocapillaris has been implicated in the progression of AMD. In advanced nonneovascular AMD, geographic atrophy (GA) is associated with loss of photoreceptors, RPE, and the choriocapillaris. Whether the RPE or choriocapillaris alterations are the primary event in pathogenesis has been a matter of debate (26). Histologic studies have described choriocapillaris dysfunction in the intermediate stage of AMD, before development of GA or choroidal neovascularization (27, 28). Whereas efforts have been made to assess the choriocapillaris in vivo (29), its small size, high density, and high permeability have made it difficult for conventional imaging modalities, including FA and ICG, to provide meaningful assessment. By segmenting a layer extending 10 μm posterior to Bruch's membrane, OCT angiography provides qualitative and quantitative evaluation of the choriocapillaris, which may be valuable in understanding its role in AMD.

OCT angiography has utility in elucidating the state of the choriocapillaris in GA (Fig. 5). In a patient with perifoveal GA, the fundus photograph (Fig. 5*A*) and autofluorescence image (Fig. 5*B*) show the affected region. The drusen–RPE complex thickness map (the axial distance from the apex of the drusen and the RPE layer to BM, Fig. 5*C*) shows an area of RPE loss corresponding to the clinically evident GA. The choriocapillaris flow is absent in most of the area correlating to clinical GA (Fig. 5 *E* and *F*). Prior histopathological findings (27) showed that viable choriocapillaris can exist in areas of GA, but highly constricted. OCT angiography is based on flow detection; therefore, constricted choriocapillaris with little or no flow may appear absent. In some areas near the border of the GA with RPE loss, intact choriocapillaris flow is present (Fig. 5 *G* and *H*). In this area of preserved choriocapillaris and slightly beyond it, the outer nuclear layer is also preserved; however, in most of the GA area, the outer nuclear layer, photoreceptors, and RPE are absent.

Choriocapillaris Loss in Choroideremia. Pathology of the choriocapillaris has been implicated in many disease processes apart from AMD, including those with genetic, inflammatory, and infectious etiologies. Choroideremia is an X-linked recessive chorioretinal dystrophy associated with mutation of the *CHM* gene. This gene encodes the Rab escort protein 1 (REP-1) and is characterized by significant atrophy of the RPE and choriocapillaris with photoreceptor loss (30). Affected patients typically experience night blindness in their first or second decade, followed by constriction of the peripheral visual fields until central vision is lost. Patients with choroideremia often demonstrate retinal vessels of normal caliber until late in the disease, suggesting a relatively greater loss of choroidal blood flow (30). Spectral-domain OCT studies of

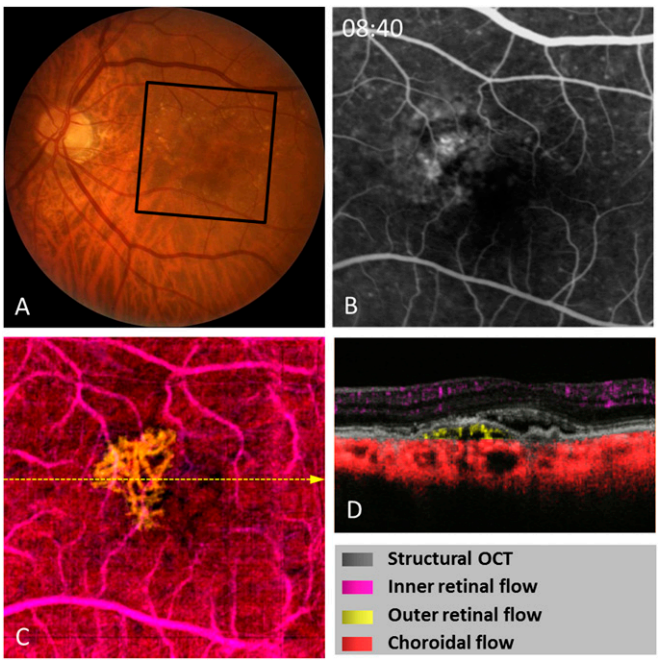

Fig. 4. Type I CNV case imaged by a 100-kHz swept-source OCT system with a center wavelength of 1,050 nm. The CNV is identified by OCT angiography (3 × 3 mm), but it is ill defined by fluorescein angiography (FA). (*A*) Fundus photograph. The black square outlines the areas shown on the angiograms. (*B*) Late stage fluorescein angiograph showing an occult CNV. (*C*) Composite en face color-coded OCT angiogram with CNV flow highlighted in yellow. The CNV area was 0.96 mm^2 and the outer retina flow index was 0.012. The yellow dashed line indicates the position of the OCT cross-section. (*D*) Cross-sectional color OCT angiogram. Both composite en face (*C*) and cross-sectional color OCT angiograms (*D*) show inner retinal flow in purple, outer retinal flow (CNV) in yellow, and choroidal flow in red. The CNV is predominantly under the RPE.

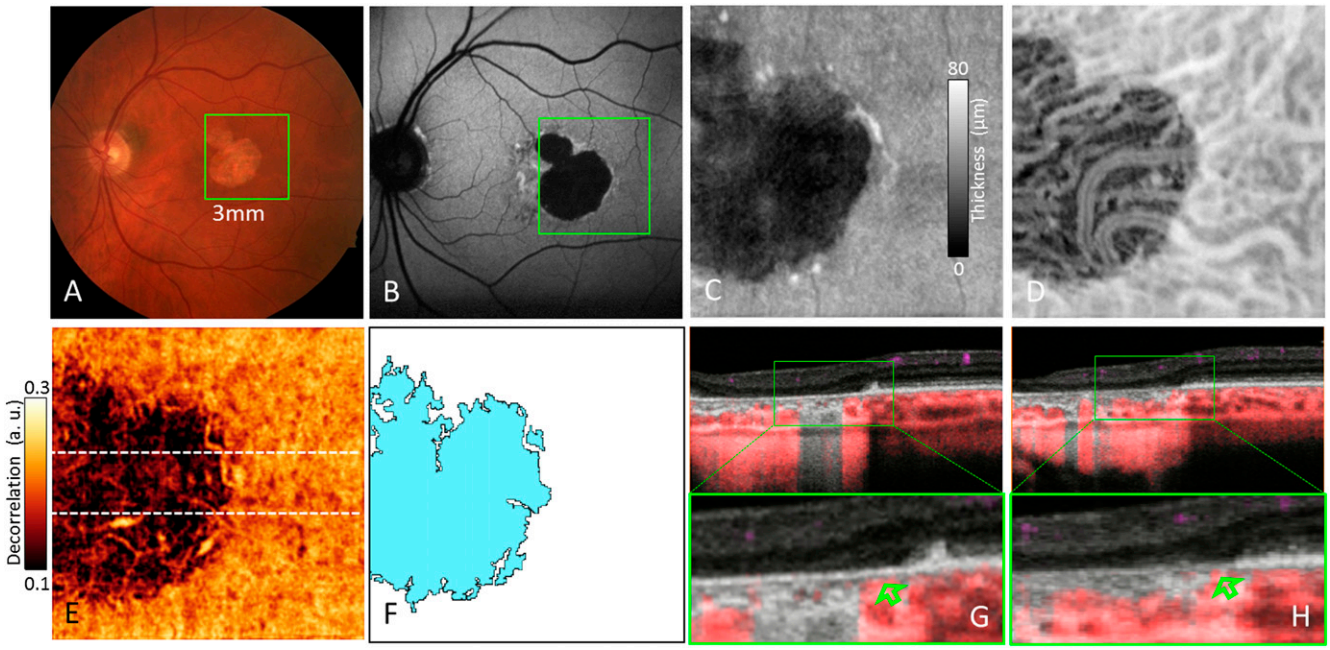

Fig. 5. Geographic atrophy case imaged by a 100-kHz swept-source OCT system with a center wavelength of 1,050 nm. (*A*) Fundus photograph showing the area of geographic atrophy (GA) adjacent to the foveal center. (*B*) An autofluorescence image sharply outlines the area of absent RPE and is surrounded by a halo of hyperautofluorescence. The green squares in *A* and *B* outline the area shown in *C*–*F*. (*C*) A drusen–RPE complex thickness map shows the area of RPE thinning (the dark area nasally). (*D*) An en face OCT structural image on an inverse gray scale of the deeper choroid reveals medium- and large-sized vessels. (*E*) An en face OCT angiogram (3 × 3 mm) of the choriocapillaris shows dramatically decreased, but not absent, choriocapillaris flow in the area of GA. (*F*) The light blue color represents the choriocapillaris nonperfusion area (2.75 mm^2). (*G* and *H*) Cross-sectional composite OCT angiograms show the absence of choriocapillaris flow in most of the area of GA, but the flow at the edge of the atrophy is spared (shown by the green arrows in the magnified views).

patients with choroideremia show photoreceptor rosettes, suggesting loss of RPE before that of photoreceptors. However, the temporal relationship of RPE loss versus choriocapillaris loss is unknown.

OCT angiography with SSADA may aid in understanding the disease pathogenesis and inform the debate on whether degeneration occurs first in the choriocapillaris, RPE, or photoreceptors. En face OCT angiography has the ability to map both retinal and choroidal perfusion down to the capillary level. In the three subjects with choroideremia, OCT angiography (Fig. 6) showed that the choriocapillaris nonperfusion area was more extensive than the retinal nonperfusion in all cases. The area of RPE loss was even more extensive than choriocapillaris nonperfusion. These patterns suggest that RPE loss might be the primary event, with subsequent choroidal perfusion loss following more closely than retinal perfusion loss. With the recent initiation of gene therapy trials (31), the ability to quantify and map both choroidal and retinal circulations may prove valuable in assessing disease severity and response to treatment.

Discussion

The cases presented in this article show the potential clinical applications of OCT angiography for noninvasive vascular imaging in the eye. Although clinical studies using OCT angiography have investigated polypoidal choroidal vasculopathy (32), macular degeneration (33, 34), diabetic retinopathy (35), and macular telangiectasia type 2 (36, 37), they were descriptive in nature. In this study, a comprehensive OCT angiography system was demonstrated that includes scanning, flow detection, segmentation, display, and quantification. There are several important contributions in this report. First, OCT angiography with SSADA is able to capture a large 6 × 6 mm view of the macula with adequate resolution using a commercially available OCT system. Second, the multicolor display system shows multiple circulations in the same image panel so that the location of pathologies can be located in relation to the retinal vasculature with minimal interference from flow projection artifacts. Third, quantification of RNV and quantification of the area of capillary dropout in the retinal circulation and choriocapillaris are also shown in vivo for the first time to our knowledge.

OCT angiography differs from FA, in which ocular pathology is typically highlighted by leakage and staining. On OCT angiography, ocular pathologies are identified by the abnormal presence of flow in layers that usually lack blood vessels or the absence of flow in normally vascular layers. Because dye leakage and staining do not occur in OCT angiography, the boundaries, and therefore areas, of capillary dropout and neovascularization can be measured without these complications. OCT angiography has several other compelling characteristics that make it a promising modality for clinical use. OCT angiography using SSADA can be acquired in a few seconds, a dramatic improvement compared with several minutes for FA. Its 3D nature allows separate evaluation of abnormalities in retinal and choroidal circulations. Additionally, quantitative information, such as vessel density, flow index, and nonperfusion areas, can now be obtained. OCT angiography might be useful in assessing the response of CNV to antiangiogenic treatment by quantifying the size and flow index of CNV before and after therapy. Furthermore, the scan pattern and SSADA processing can be implemented on spectral-domain or swept-source OCT systems without any special hardware modification, provided that imaging speeds are sufficient; i.e., ≥70 kHz is required to provide 6 × 6 mm angiograms with capillary details within a reasonable scan time (≤3 s).

OCT angiography has several limitations and requirements. First, projection artifacts are observed on the cross-sectional angiograms. These artifacts are due to fluctuating shadows cast by flowing blood in large inner retinal vessels that cause variation in the OCT signal from deeper layers. The projection artifact

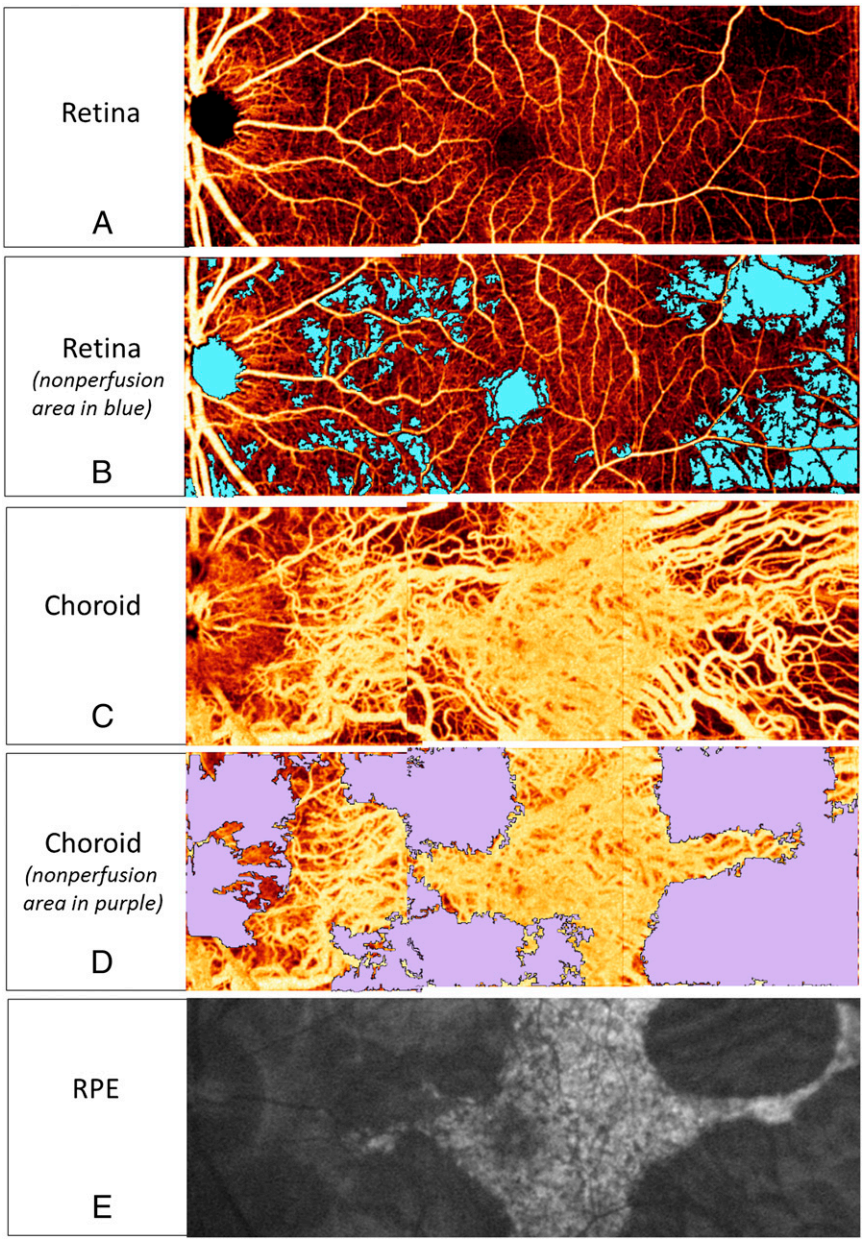

Fig. 6. Choroideremia case imaged by a 100-kHz swept-source OCT system with a center wavelength of 1,050 nm. The large-field en face OCT angiograms (~3 × 8.5 mm) were produced by stitching together three 3 × 3 mm scans. (*A*) OCT angiography of inner retinal blood flow. (*B*) OCT angiography with quantification of inner retinal blood flow demonstrating patchy areas of nonperfusion (blue) in the extrafoveal macula. The total nonperfusion area of the inner retina was 7.65 mm^2. (*C*) OCT angiography of the choroidal blood flow, including choriocapillaris and deep choroid. It should be noted that OCT angiography is able to image deeper choroidal vessels in this case due to the relative absence of the overlying choriocapillaris and RPE. (*D*) OCT angiography of the choroidal blood flow with quantification of the choriocapillaris nonperfusion area (purple), which was 12.11 mm^2 (47.5% of image area). (*E*) An autofluorescence image outlines the area of existing RPE (hyperautofluorescent area).

from the retinal circulation can be easily removed from the en face views of deeper layers because the retinal vasculature is relatively sparse. However, the choriocapillaris is nearly confluent, and its shadow often obscures OCT angiography visualization of deeper choroidal vessels. Second, the flow signal fadeout in large vessels with very fast blood flow can induce fringe washout of OCT signals (16). This means that central retinal vessels in the disk and large vessels in the deep choroid cannot be visualized using SSADA. However, we can use an inverted signal scale to take advantage of fringe washout to visualize deep choroidal vessels. Third, decorrelation (flow signal) is linearly related to velocity over a limited range. A higher decorrelation value thus implies higher velocity flow. This range is dependent on the time scale of the SSADA measurement. With a 70-kHz spectral OCT system and 200+ A-scans per cross-sectional B-scan, SSADA should be sensitive to the normal capillary flow speeds, which have been estimated at between 0.4 and 3 mm/s (38, 39). If blood flow is extremely slow in pathological conditions, the decorrelation values may be below noise background, in which case flow would not be detected by OCT angiography. In larger vessels with higher velocities, the SSADA signal reaches a maximum value (saturates). This suggests that the angiography-based flow index, at current scan speeds, is a mixed measure of vascular density of both large and small vessels plus a

component of capillary flow velocity. Fourth, unlike FA, OCT angiography cannot visualize dye leakage. However, the visualization of intraretinal and subretinal fluid accumulation on structural OCT may provide information associated with fluid leakage (40), whereas CNV activity may be evaluated by assessing the presence or characteristics of its perfusion (24). Fifth, the scan area is relatively small (3 × 3–6 × 6 mm). Larger area angiograms can be achieved, but it would require higher speed OCT systems that are not yet commercially available (41). Lastly, because OCT angiography identifies depth resolve pathology, practical clinical applications require automated image processing software that accurately delineates tissue layers.

In summary, OCT angiography can provide safe and repeatable (42) high-resolution images of retinal and choroidal circulations, in addition to structural OCT information. Its ability to noninvasively visualize neovascularization and nonperfusion unaffected by leakage and staining offers advantages over dye-based angiography methods. The ability to quantify perfusion and separately visualize retinal and choroidal vasculature makes it uniquely suited for a variety of research and clinical applications.

Methods

Human Subjects Imaging. Study subjects were enrolled after informed consent in accordance with an Institutional Review Board/Ethics Committee approved protocol at Oregon Health & Science University and at the Massachusetts Institute of Technology in compliance with the Declaration of Helsinki. Healthy participants or patients with a diagnosis of retinal disease (diabetic retinopathy/AMD/choroideremia) were selected from the Retina Division of the Casey Eye Institute for their clear media and ability to fixate. In total, 15 healthy subjects, 14 with diabetic retinopathy, 26 with AMD, and 3 with choroideremia were enrolled. To better demonstrate the potential clinical application of this OCT methodology, six cases with characteristic pathological and clinical features were selected for this article.

Color fundus and optic disk photographs were acquired with Zeiss fundus cameras (FF3 for Figs. 2*A1* and 4*A* and FF450 for Fig. 5; Carl Zeiss Meditec) and the Optos 200Tx confocal scanning laser ophthalmoscope (cSLO) (Fig. 3*A*; Optos PLC). For fluorescein angiography, 10% sodium fluorescein in water (500 mg/5 mL) was injected i.v. using a 23- or 25-gauge needle, followed by a flush of normal saline. Fluorescein angiography was performed using either the Optos 200Tx cSLO (Figs. 2*A2* and 3*B*) or the Spectralis HRA+OCT cSLO (Fig. 4*B*; Heidelberg Engineering). For both cSLO devices, a 488-nm wavelength laser excited the fluorescein, and a barrier filter at 500 nm separated the excitation and emission light. The fluorescein autofluorescence image in Figs. 5 and 6 was also acquired using the Spectralis HRA+OCT cSLO. These procedures, imaging systems, and contrast dyes are approved by the Food and Drug Administration.

OCT Systems. Two OCT systems were used in this study. The first was a custom-built swept-source OCT instrument (14, 24, 42, 43). The device operated at an axial scan rate of 100 kHz using a swept-source cavity laser operating at ∼1,050 nm with a sweep range of 100 nm. The instrument has a 5.3-μm axial resolution and 18-μm lateral resolution with an imaging range of 2.9 mm in tissue. The ocular light exposure was 1.9 mW, which was within the American National Standards Institute safety limit (44). The second OCT system was a commercial spectral domain OCT instrument (RTVue-XR; Optovue) (36). The center wavelength was ∼840 nm with a full-width half-maximum bandwidth of 45 nm and an axial scan rate of 70 kHz.

OCT Imaging. A 3 × 3 or 6 × 6 mm scanning area was used for OCT angiography. In the fast transverse scanning direction, 200 axial scans were sampled to obtain a single B-scan. Multiple repeated B-scans (eight for the swept-source OCT and five for the spectral OCT), were captured at a fixed position before proceeding to the next sampling location. A total of 200 locations along a 3- or 6-mm distance in the slow transverse direction were sampled to form a 3D data cube. For the swept-source system, with a B-scan frame rate of 455 frames per second, the 1,600 B-scans in each scan were acquired in ∼3.5 s. Four volumetric raster scans, including two horizontal priority fast transverse (*x*-fast) scans and two vertical priority fast transverse (*y*-fast) scans, were obtained consecutively in one session. For the spectral domain OCT system, with a B-scan frame rate of 320 frames per second, the 1,000 B-scans in each scan were acquired in ∼3.1 s. Two volumetric raster scans including one *x*-fast scan and one *y*-fast scan were obtained.

SSADA Processing. The SSADA algorithm was used to distinguish blood flow from static tissue as described in detail in a previous publication (14). By calculating the decorrelation of the signal amplitude from consecutive B-scans, contrast between static and nonstatic tissue is created that enables visualization of blood flow. Decorrelation is a mathematical function that quantifies variation without being affected by the average signal strength, as long as the signal is strong enough to predominate over optical and/or electronic noise. Specifically, the algorithm splits the OCT image into different spectral bands, thus increasing the number of usable image frames. In the optimized SSADA technique, the OCT signal is first split into 11 spectral bands to obtain 11 low axial resolution images instead of a single image frame with high axial resolution. Each new frame has a lower axial resolution that is less susceptible to axial eye motion caused by retrobulbar pulsation. This lower resolution also translates to a wider coherence gate over which reflected signal from a moving particle such as a blood cell can interfere with adjacent structures, thereby increasing speckle contrast. In addition, each spectral band contains a different speckle pattern and independent information on flow. When amplitude decorrelation images from multiple spectral bands are combined, the flow signal is increased. By enhancing the flow signal and suppressing bulk motion noise, SSADA improves the signal-to-noise ratio of flow detection by at least a factor of two (14). Motion artifacts were further corrected and the flow signal increased by applying an image registration algorithm that registered orthogonal raster-scanned volumes (45).

OCT Angiogram Visualization and Quantification. To enhance visualization, the 3D angiogram was separately projected as en face views in five layers: vitreous, inner retina, outer retina, choriocapillaris, and deep choroid (Fig. 1). The separated en face OCT angiography images were presented in a sepia color scale. A composite view was created, where each layer was assigned a different color. The color-coded angiogram can be superimposed on a gray-scale, cross-sectional, structural OCT image to demonstrate blood flow and structural information simultaneously. Flow projection artifacts are a common problem for existing OCT angiography techniques (3–13). To better distinguish and interpret the blood flow within different layers, a negative filter was used to mask projection artifacts from the larger caliber retinal vessels (24).

To quantify the blood flow within the regions of interest, the flow index, vessel density, and neovascularization area were determined from the en face maximum projection angiogram. The flow index was calculated as the average decorrelation value (which is correlated with flow velocity) in the selected region, and the vessel density was calculated as the percentage area occupied by vessels and microvasculature in the selected region. For scans of the macula, flow index and vessel density can be routinely determined for the parafovea and/or perifovea. The parafovea is defined to be an annular region with an inner diameter of 0.6 mm and outer diameter of 2.5 mm centered on the FAZ. The perifovea is defined to be the annular region extending from the edge of the parafovea to an outer diameter of 5.5 mm. For a 3 × 3 mm scan, only the parafovea values can be determined. Examples from macular angiograms are shown in Fig. 2 *C1* and *C2*. The vitreous or outer retinal flow index can be used to indicate the RNV or CNV flow within the scanned area (3 × 3 or 6 × 6 mm) of the vitreous or outer retina. The retinal or choroidal neovascularization area was the area occupied by vessels in the vitreous or outer retina. To identify and quantify the capillary dropout of the inner retina or choriocapillaris, the nonperfusion map was created by identifying decorrelation values lower than a set cutoff point, typically 2.33 SD below the mean according to the normal distribution. Morphologic operations were then used to remove areas below a certain size to reduce noise. The remaining areas were then summed and converted from pixels to metric units.

ACKNOWLEDGMENTS. This work was supported by National Institutes of Health Grants R01-EY023285, R01-EY024544, DP3 DK104397, R01-EY11289, K08-EY021186, T32-EY23211, and P30-EY010572; Clinical and Translational Science Award Grant UL1TR000128; unrestricted Grant and Career Development Award CD-NMT-0914-0659-OHSU from Research to Prevent Blindness; enhanced Career Development Award AFOSR FA9550-10-1-0551 from Foundation Fighting Blindness; and German Research Foundation Grants DFG-HO-1791/11-1 and DFG-GSC80-SAOT.

1. Congdon N, et al.; Eye Diseases Prevalence Research Group (2004) Causes and prevalence of visual impairment among adults in the United States. *Arch Ophthalmol* 122(4):477–485.

2. López-Sáez MP, et al. (1998) Fluorescein-induced allergic reaction. *Ann Allergy Asthma Immunol* 81(5 Pt 1):428–430.

3. Wang RK, et al. (2007) Three dimensional optical angiography. *Opt Express* 15(7): 4083–4097.
4. Grulkowski I, et al. (2009) Scanning protocols dedicated to smart velocity ranging in spectral OCT. *Opt Express* 17(26):23736–23754.
5. Yu L, Chen Z (2010) Doppler variance imaging for three-dimensional retina and choroid angiography. *J Biomed Opt* 15(1):016029.
6. Makita S, Jaillon F, Yamanari M, Miura M, Yasuno Y (2011) Comprehensive in vivo micro-vascular imaging of the human eye by dual-beam-scan Doppler optical coherence angiography. *Opt Express* 19(2):1271–1283.
7. Zotter S, et al. (2011) Visualization of microvasculature by dual-beam phase-resolved Doppler optical coherence tomography. *Opt Express* 19(2):1217–1227.
8. Braaf B, Vermeer KA, Vienola KV, de Boer JF (2012) Angiography of the retina and the choroid with phase-resolved OCT using interval-optimized backstitched B-scans. *Opt Express* 20(18):20516–20534.
9. Mariampillai A, et al. (2008) Speckle variance detection of microvasculature using swept-source optical coherence tomography. *Opt Lett* 33(13):1530–1532.
10. Motaghiannezam R, Fraser S (2012) Logarithmic intensity and speckle-based motion contrast methods for human retinal vasculature visualization using swept source optical coherence tomography. *Biomed Opt Express* 3(3):503–521.
11. Enfield J, Jonathan E, Leahy M (2011) In vivo imaging of the microcirculation of the volar forearm using correlation mapping optical coherence tomography (cmOCT). *Biomed Opt Express* 2(5):1184–1193.
12. Fingler J, Zawadzki RJ, Werner JS, Schwartz D, Fraser SE (2009) Volumetric microvascular imaging of human retina using optical coherence tomography with a novel motion contrast technique. *Opt Express* 17(24):22190–22200.
13. Liu G, Lin AJ, Tromberg BJ, Chen Z (2012) A comparison of Doppler optical coherence tomography methods. *Biomed Opt Express* 3(10):2669–2680.
14. Jia Y, et al. (2012) Split-spectrum amplitude-decorrelation angiography with optical coherence tomography. *Opt Express* 20(4):4710–4725.
15. Mrejen S, Spaide RF (2013) Optical coherence tomography: Imaging of the choroid and beyond. *Surv Ophthalmol* 58(5):387–429.
16. Hendargo HC, McNabb RP, Dhalla A-H, Shepherd N, Izatt JA (2011) Doppler velocity detection limitations in spectrometer-based versus swept-source optical coherence tomography. *Biomed Opt Express* 2(8):2175–2188.
17. Frank RN (2004) Diabetic retinopathy. *N Engl J Med* 350(1):48–58.
18. Antonetti DA, Klein R, Gardner TW (2012) Diabetic retinopathy. *N Engl J Med* 366(13): 1227–1239.
19. Group ETDRSR; Early Treatment Diabetic Retinopathy Study Research Group (1991) Classification of diabetic retinopathy from fluorescein angiograms. ETDRS report number 11. *Ophthalmology* 98(5, Suppl):807–822.
20. Group DRSR; The Diabetic Retinopathy Study Research Group (1981) Photocoagulation treatment of proliferative diabetic retinopathy. Clinical application of Diabetic Retinopathy Study (DRS) findings, DRS Report Number 8. *Ophthalmology* 88(7): 583–600.
21. Ambati J, Ambati BK, Yoo SH, Ianchulev S, Adamis AP (2003) Age-related macular degeneration: Etiology, pathogenesis, and therapeutic strategies. *Surv Ophthalmol* 48(3):257–293.
22. Hee MR, et al. (1996) Optical coherence tomography of age-related macular degeneration and choroidal neovascularization. *Ophthalmology* 103(8):1260–1270.
23. Gass J (1997) *Stereoscopic Atlas Of Macular Diseases: Diagnosis and Management* (Mosby, St. Louis), Ed 4, pp 24–26.
24. Jia Y, et al. (2014) Quantitative optical coherence tomography angiography of choroidal neovascularization in age-related macular degeneration. *Ophthalmology* 121(7):1435–1444.
25. Ying GS, et al.; Comparison of Age-related Macular Degeneration Treatments Trials Research Group (2013) Baseline predictors for one-year visual outcomes with ranibizumab or bevacizumab for neovascular age-related macular degeneration. *Ophthalmology* 120(1):122–129.
26. Bhutto I, Lutty G (2012) Understanding age-related macular degeneration (AMD): Relationships between the photoreceptor/retinal pigment epithelium/Bruch's membrane/choriocapillaris complex. *Mol Aspects Med* 33(4):295–317.
27. McLeod DS, et al. (2009) Relationship between RPE and choriocapillaris in age-related macular degeneration. *Invest Ophthalmol Vis Sci* 50(10):4982–4991.
28. Mullins RF, Johnson MN, Faidley EA, Skeie JM, Huang J (2011) Choriocapillaris vascular dropout related to density of drusen in human eyes with early age-related macular degeneration. *Invest Ophthalmol Vis Sci* 52(3):1606–1612.
29. Grunwald JE, Metelitsina TI, Dupont JC, Ying G-S, Maguire MG (2005) Reduced foveolar choroidal blood flow in eyes with increasing AMD severity. *Invest Ophthalmol Vis Sci* 46(3):1033–1038.
30. Coussa RG, Traboulsi EI (2012) Choroideremia: A review of general findings and pathogenesis. *Ophthalmic Genet* 33(2):57–65.
31. MacLaren RE, et al. (2014) Retinal gene therapy in patients with choroideremia: Initial findings from a phase 1/2 clinical trial. *Lancet* 383(9923):1129–1137.
32. Miura M, Makita S, Iwasaki T, Yasuno Y (2011) Three-dimensional visualization of ocular vascular pathology by optical coherence angiography in vivo. *Invest Ophthalmol Vis Sci* 52(5):2689–2695.
33. Kim DY, et al. (2013) Optical imaging of the chorioretinal vasculature in the living human eye. *Proc Natl Acad Sci USA* 110(35):14354–14359.
34. Moult E, et al. (2014) Ultrahigh-speed swept-source OCT angiography in exudative AMD. *Ophthalmic Surg Lasers Imaging Retina* 45(6):496–505.
35. Schwartz DM, et al. (2014) Phase-variance optical coherence tomography: A technique for noninvasive angiography. *Ophthalmology* 121(1):180–187.
36. Spaide RF, Klancnik JM, Jr, Cooney MJ (2014) Retinal vascular layers in macular telangiectasia type 2 imaged by optical coherence tomographic angiography. *JAMA Ophthalmol* 133(1):66–73.
37. Thorell M, et al. (2014) Swept-source OCT angiography of macular telangiectasia type 2. *Ophthalmic Surg Lasers Imaging Retina* 45(5):369–380.
38. Riva CE, Petrig B (1980) Blue field entoptic phenomenon and blood velocity in the retinal capillaries. *J Opt Soc Am* 70(10):1234–1238.
39. Tam J, Tiruveedhula P, Roorda A (2011) Characterization of single-file flow through human retinal parafoveal capillaries using an adaptive optics scanning laser ophthalmoscope. *Biomed Opt Express* 2(4):781–793.
40. Drexler W, Fujimoto JG (2008) State-of-the-art retinal optical coherence tomography. *Prog Retin Eye Res* 27(1):45–88.
41. Blatter C, et al. (2012) Ultrahigh-speed non-invasive widefield angiography. *J Biomed Opt* 17(7):070505.
42. Jia Y, et al. (2014) Optical coherence tomography angiography of optic disc perfusion in glaucoma. *Ophthalmology* 121(7):1322–1332.
43. Choi W, et al. (2013) Choriocapillaris and choroidal microvasculature imaging with ultrahigh speed OCT angiography. *PLoS ONE* 8(12):e81499.
44. Anonymous (2007) *American National Standard for Safe Use of Lasers, ANSI Z136 Series* (American National Standards Institute, New York).
45. Kraus MF, et al. (2012) Motion correction in optical coherence tomography volumes on a per A-scan basis using orthogonal scan patterns. *Biomed Opt Express* 3(6):1182–1199.